Studies in the BNL 21-GeV/c negative-hyperon beam. I. Σ and Ξ production and asymmetry in the decay $\Xi^- \to \Lambda\pi^-$

W. E. Cleland, W. E. Cooper, M. Dris,* E. Engels, Jr., M. L. Herbert,† D. E. Kraus, and J. A. Thompson
University of Pittsburgh, Pittsburgh, Pennsylvania 15260

D. Lowenstein
Brookhaven National Laboratory, Upton, New York 11973

(Received 10 July 1979)

In the Brookhaven National Laboratory 20.8-GeV/c negative-hyperon beam, we have measured the production ratios Σ^-/π^-, Ξ^-/π^-, and Σ^-/Ξ^- by 29.4-GeV/c protons incident on Al and Al_2O_3 targets. We have also measured the asymmetry parameter in the decay $\Xi^- \to \Lambda\pi^-$ and find $\alpha_{\Xi^-} = -0.49 \pm 0.04$.

I. INTRODUCTION

This is Part I of a two-part report on experiments in the Brookhaven National Laboratory charged-hyperon beam. In this part we report on the nonleptonic-decay results: production rates for negative Σ's, pions, and cascade hyperons Ξ, and α_{Ξ^-}, the decay parameter in $\Xi^- \to \Lambda\pi^-$ decay. These results have interest in themselves, and they also serve as calibrations for the leptonic processes which motivated the experiment.

In this experiment we have obtained a sample of 17000 normal cascade decays, reconstructed in a sample in which a downstream Čerenkov counter was required in the trigger and another sample of 9046 events with no such trigger bias. The two samples give consistent values of α_{Ξ^-}. Our large sample allows us to study possible systematic errors carefully, but we prefer to quote the value derived from the unbiased sample. This value is $\alpha_{\Xi^-} = -0.49 \pm 0.04$, consistent with the world averages of measurements of α_{Ξ^-} and α_{Ξ^0}.

II. BEAM AND APPARATUS

The apparatus used in this experiment is shown in Fig. 1. It was designed primarily to detect leptonic decays of hyperons, but nonleptonic decays were detected with comparable efficiency. Decay modes searched for were

$$\Sigma^- \to n\pi^-, \tag{1}$$

$$\Sigma^- \to ne^-\bar{\nu}_e, \tag{2}$$

$$\Xi^- \to \Lambda^0\pi^-, \tag{3}$$

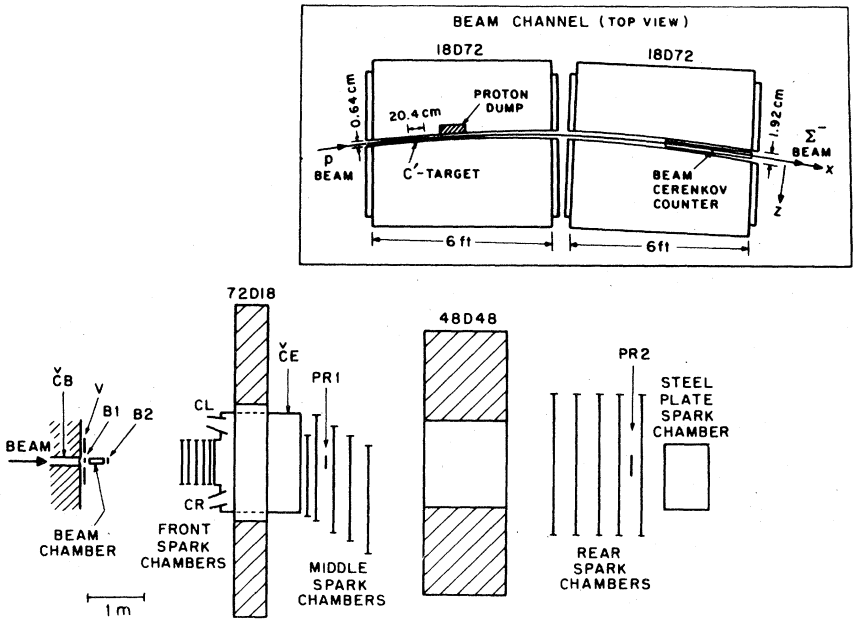

FIG. 1. Plan view of the apparatus and the hyperon channel.

$$\Xi^- \to \Lambda^0 e^- \bar{\nu}_e , \quad (4)$$

$$\Xi^- \to \Lambda^0 \mu^- \bar{\nu}_\mu , \quad (5)$$

$$\Xi^- \to \Sigma^0 e^- \bar{\nu}_e . \quad (6)$$

In this paper we discuss the detection of the nonleptonic processes, Eqs. (1) and (3). The other decay modes are discussed in paper II.[1]

The hyperons were produced, together with a much larger number of nonstrange particles, by the interaction of a part of the Brookhaven alternating-gradient synchroton (AGS) external proton beam (29.4 GeV/c) (10^{11} protons/AGS pulse) with C', an aluminum oxide or aluminum target 2.5 mm wide, 5.0 mm high, and 254 mm (about one interaction length) long. High-momentum negative particles (20.8 ± 2.1 GeV/c) produced near the forward direction were selected by a narrow curved channel through a pair of 18D72 magnets (insert, Fig. 1). The metals forming the channel and the magnet core stopped those primary protons which did not interact in C', and contained most of the subsequent hadronic and electromagnetic showers.

The proton intensity was adjusted to produce a flux of 3×10^4 beam particles from the channel each AGS pulse. This predominantly pion beam contained about 260 Σ^- and about 6 Ξ^-. Two small scintillators in coincidence ($B1$ and $B2$) identified a beam particle emerging from the channel. Baryons were selected by using the downstream half of the channel, lined with reflective coating and filled with Freon 12, as a Čerenkov counter ($\check{C}B$) in anticoincidence. The momentum of the beam particles was measured to 1% by making use of the excellent resolution [0.2 mm full width at half maximum (FWHM)] of the eight-plane high-pressure magnetostrictive spark chamber positioned between $B1$ and $B2$. Full descriptions of the design and performance of the hyperon channel and the high-pressure chamber have been given by their designers.[2,3]

A flux of muons ($10^7/m^2$ sec) emerged from the downstream face of the channel. A (30 cm × 30 cm) scintillator (V) with a hole (2.5 cm × 2.5 cm) for the passage of the hyperon beam vetoed triggers accompanied by a charged particle in this counter.

A decay region extending 1.2 m along the beam line followed $B2$. The charged decay products were detected in three groups of magnetostrictive spark chambers (front, middle, rear) interleaved with two hodoscope magnets (a 72D18 with 61-cm gap and a 48D48 with 91.4-cm gap). Scintillators PR1 and PR2 intercepted most of the trajectories of protons from Λ decay, and were required in coincidence in triggers for decay modes involving Λ's.

Each spark-chamber group consisted of five chambers, two of which were rotated by 20° to resolve ambiguities in pairing horizontal and vertical readouts. The construction of the chambers and their high-voltage pulsing arrangements are based upon methods described in Ref. 4, except that the two wire planes on each chamber are wound orthogonally, and each chamber has its own mechanical frame and gas envelope. The magnetostrictive pulses for chambers in the front and middle groups were sensed at both ends of the delay line, which aided in recognizing spark pairs lying closer than the measured spark-pair resolution of the wands (2.5 mm) or the minimum separation for freedom from distortion (5.0 mm). Gas composition (89% Ne, 10% He, 1.2% spectroscopic grade isopropyl alcohol) was maintained by an LBL recirculation system.[5] Close control of the alcohol concentration was essential for achieving the observed spark dispersion (0.8 mm FWHM). Gas quality was adequately monitored with a simple discharge device. Clearing-field voltages were set to reduce single-spark efficiency to 50% for a track preceding the triggering event by 200 nsec.

The magnetostrictive pulses were sensed and amplified at each wand and sent to discriminator/center-finding modules. The zero-crossing point of the integral of the tripolar pulse established spark timing. Access to the center-finding circuit was gated by a discriminator for minimum spark-pulse size. Pulse thresholds were set individually for each readout and electronically varied to compensate for the 50% signal attenuation on the long wands of the rear group. Successive pulses from this module arriving at a CAMAC time digitizer[6] caused the contents of a scaler counting a 40-MHz clock to be copied into sequential locations in a 16-word memory. This allowed readout of two fiducial markers and up to 14 sparks.

The transverse coordinates of fiducial wires were established by survey to an accuracy of 0.33 mm. The positions of the spark-chamber planes along the beam direction were determined to an accuracy of 0.2 mm. The survey result agreed to this accuracy with a measurement of fiducial separations using the magnetostrictive wands calibrated on a pair of test pulse wires whose separation was carefully measured.

Departures from linearity caused by hodoscope-magnet fringe fields and the materials used to shield wands from them were found to be negligible. This was established by the reconstruction of data taken with the magnets turned off and by observing the digitized intervals for signals induced by a test rig of pulsed wires while the wands were in position on the chambers. Regular restoration of the bias magnetic field in several of the magnetostrictive wires was required to prevent degradation of the sonic-pulse waveforms and consequent loss of resolution.

The vertical component of the magnetic field was measured at several thousand points for each magnet with a flip coil. These measurements were fitted using a procedure[7] which modeled the magnet as a collection of elementary magnetic-field sources whose strengths were adjusted to optimize the fit to the measured points. For both magnets the fitted and measured fields agreed to 0.1% in the central region and to better than 2% in the corners. This technique assured that the fitted field fell off accurately at large distances from the magnet, and gave reliable values for the unmeasured components.

Simple interpolating functions giving the dependence of line integrals of field components on particle trajectory were incorporated in fast subroutines for calculating transfer characteristics of the magnets. These subroutines, used in the reconstruction and fitting programs, gave estimates of the momentum which agreed with those found from exact ray-tracing to within 0.5% for tracks with momenta between 0.5 and 1.0 GeV/c and with better accuracy at higher momenta.

The beam-channel central momentum (20.8 ± 0.6 GeV/c) was determined from the momenta of beam tracks in the spectrometer magnets. The uncertainty arises from uncertainty in absolute position of target, magnets, and spark chambers, as well as magnetic-field effects on sparks and magnetostrictive wands.

A steel-plate optical chamber located behind the rear group searched for γ rays from the decay mode of Σ^0 in Eq. (6). An air Čerenkov counter ($\check{C}E$) located inside the 72D18 identified electrons from decay modes (2), (4), and (6). The properties and performance of $\check{C}E$ and the γ-ray detector are presented in paper II.

III. DATA COLLECTION

Data were collected for several types of triggers. The rates of these triggers per AGS pulse, along with an indication of their objective, are as follows: Beam tracks ($F \cdot V = B1 \cdot B2 \cdot V$, about 3×10^4 pulse) are primarily high-momentum pions emerging from the hyperon channel and traversing the apparatus with little bending and no decay. They are useful in aligning spark chambers, and as normalization for the Σ^- and Ξ^- fluxes. Hyperon triggers ($Y \cdot V = F \cdot V \cdot \overline{\check{C}B}$, about 275/pulse) are primarily Σ and cascade but they include a few beam tracks for which $\check{C}B$ was inefficient A cascade trigger ("Ξ" $= Y \cdot V \cdot$ PR1 $\cdot$ PR2, about 5/pulse) was a hyperon in coincidence with a high-momentum positive particle as determined by counters PR1 and PR2. An event satisfying this trigger was nominally reaction (3) followed by a Λ^0 decay in a charged mode.

We also accumulated a large sample of data taken with Ξ_β triggers ($\Xi_\beta =$ "Ξ" $\cdot \check{C}E$, about 1/pulse). These triggers are used primarily for the data presented in paper II, but we make some use of them in this paper in estimating systematic uncertainties.

For any trigger involving Y, roughly $\frac{2}{3}$ of the data are from hyperon decays upstream of the fiducial region. For events in which a vertex lies within the fiducial region, about $\frac{1}{3}$ are from processes with incident Σ or pion.

Our data were collected during three periods of approximately equal running time, referred to as periods A, B, and C.

During data collection, one hour each day was allocated to normalization data: 1000 $F \cdot V$ triggers, 1000 $Y \cdot V$ triggers, and 1000 "Ξ" triggers. In addition to the calibration data, up to 10000–15000 Ξ_β triggers were collected each day. Every third day larger samples of both $Y \cdot V$ and "Ξ" triggers (3000 of each) were taken. At the end of each run, a photograph was taken of optical scalars, which was later compared with the blind CAMAC scalars that were read after each event and recorded on magnetic tape. Scalar rates were constantly monitored to reduce time lost due to electronic or detector malfunctions. The settings of the beam-transport magnets, the beam-spot size on the C' target, and the opening of the primary-beam collimator were checked about once every two hours. High voltages on the photomultiplier tubes were checked daily. The instantaneous rate in one of the beam counters was monitored electronically by requiring that the integral of the discriminator output pulse (integration time of 1 msec) remain below a preset level in order to enable data collection.

A PDP-15 computer read in the data for each trigger, performed some rough checks on the data, deleted invalid sparks from the digitizer readout, and recorded the data on magnetic tape. The data acquisition program has been described in detail elsewhere.[8] Off-line reconstruction of part of our data was carried out on the Brookhaven PDP-10 computer at the on-line data facility. This program provided pulse height and timing distributions for critical counters, spark-chamber efficiencies and resolutions, and the yield of reconstructed Λ's and cascades.

IV. DATA REDUCTION

A. Programs

The data tapes were processed through three programs on the University of Pittsburgh DEC-10 system. The first program, TOPSY, was a pat-

tern recognition program that grouped sparks on a straight line within each cluster of spark chambers. The second program, GRIST, used the tracks to make geometrical and kinematic fits to reaction (3). The third program, POSTAN, performed the selection of the final data sample and produced the distributions of interest.

TOPSY, which identified line segments from sparks, began by considering the sparks from only one end of a wand. The criterion for a track to be established was that a minimum of six sparks from a straight line (out of ten possible sparks in the downstream chambers or eight in the beam chamber). If a line was formed from the YZ coordinates we required at least five YZ points and one UV point or four YZ points and two UV points. If a line was formed from the two UV chambers in a cluster, it tried every possible combination of two sparks and looked for confirmation in the YZ chambers for a total of at least six sparks.

To minimize the number of bad lines found and to reduce computer time, a number of cuts were made in TOPSY. All the sparks had to lie in a fiducial region appropriate to a β-decay topology, which is larger than the fiducial volume for reaction (3). In order to be included in the collection of sparks defining a track, a spark had to be within a specified tolerance from a line formed by four of the other sparks on the track. The tolerances range from 0.5 mm in the high-pressure chamber to $\approx$2.0 mm in the front, middle, and rear cluster. If a line was found which contained a spark from every chamber in a cluster, those sparks were not used in any other track. A number of geometric cuts were made on each line segment. The beam track was required to have a vertical slope of less than $\pm$10 mrad and a horizontal slope of less than $\pm$20 mrad to ensure that it came from the C' target and did not scatter in the channel. Tracks in the front cluster were required to pass within 38.1 cm of the beam line in both the vertical and horizontal projections. Tracks in the middle and rear chambers were required to satisfy the same criterion in the vertical projection only. All of the tracks were required to have vertical and horizontal slopes within limits set for each cluster in order to eliminate many of the accidental tracks.

The number of tracks found in each cluster was limited to twenty. If TOPSY found a larger number than this, it removed tracks with fewer sparks. After all of the lines were found, a check was made of the double-ended wands for a confirming spark. A tolerance of about 5 mm was allowed. These confirming sparks, although not used in the pattern recognition, were flagged so that GRIST could use them in fitting the tracks. An output record was written by TOPSY only when a minimum number of tracks, consistent with the topology for the type of trigger being processed, was present in each cluster. These cuts eliminated about 75% of the "Ξ" triggers and over 80% of the Ξ_β triggers. A small fraction (1%) of the events was lost because the input record was unreadable.

The program GRIST performed the geometrical and kinematic reconstruction of the events. The tracks identified by TOPSY in each cluster of chambers were first fitted to straight lines. Pairs of tracks were then formed from tracks on either side of a magnet by requiring vertical and horizontal information consistent with a possible trajectory through the magnet; the momentum was determined from the fitted trajectory. Vertices were formed from the fitted trajectories, both for the Λ (vertex from a positive and a negative trajectory in the spectrometer) and the parent beam particle (Λ plus a negative trajectory in the spectrometer). A kinematic fit was made to the Λ decay, using the fitted track parameters and the full error matrices. In general, whenever a higher-level geometrical or kinematic fit was made, the program took into account possible correlations between the variables of a previous fit by using the variance matrix from that fit. For each fit, the value of χ^2 and the number of degrees of freedom were saved for use in the selection process. Details of the procedures and cuts used are given in the data analysis sections for the specific processes.

The momenta of the tracks were determined by requiring that the trajectory calculated using the field integrals agree with the tracks observed in the chambers. In the case of beam tracks, we required that the trajectory intersect the production target. For the two downstream chambers, a "pair" was formed by joining two tracks, one on either side of the magnet. Since there was little vertical bending, their vertical slopes were required to agree within the limits given by multiple Coulomb scattering and vertical bending. The vertical-angle tolerance was $\pm(4+16/P)$ mrad, where P is measured in GeV/c. Also, the vertical position of the first track, projected to the exit of the magnet, was required to agree within 4 cm with the position of the second track. The ratio of the horizontal displacement to the change in horizontal displacement to the change in horizontal angle was required to be within limits related to the effective length of the magnet. For the 72D18, the allowed range is 80–120 cm; for the 48D48 it is 100–150 cm. If the pair passed the above vertical and horizontal cuts, a prelim-

inary estimate of the momentum of the particle was made from the difference in horizontal angles on either side of the magnet. GRIST then uses this initial momentum to trace the first track through the magnet, using the equations of motion and the field integrals, and compared the predicted exit position and angle with the coordinates of the exiting track. The parameters of the entering track and the momentum were then iteratively adjusted, consistent with the known spark-chamber resolution and uncertainty in the magnetic field (approximately 0.5%), to get the best possible fits.

A class of events which required a treatment different from that described above is those events in which the Λ decayed inside the 72D18 magnet and the proton track was seen in both the middle and rear clusters, but the pion track was seen only in the middle cluster. In this case, the pion momentum can only be determined if the position of the Λ decay vertex is known. The initial estimate of the position of this vertex was taken to be the intersection of the tracks in the vertical view. The momentum of the pion was assigned by assuming that the two particles were the decay products of a Λ. The variables in the fit are the track parameters, including the momentum, of the Λ. These were adjusted until the calculated angles and positions of the tracks exiting the 72D18 and the proton momentum fitted the measured values.

A special version of GRIST was used to determine the alignment parameters for the spark chambers. Deviations from the measured positions of the fiducial wire locations were found from fitting particle trajectories. We first used a beam pion run with the two spectrometer magnets turned off and fit to trajectories that originated at the C' target, traversed the hyperon channel, and made a straight line between the beam chamber and the rear cluster. Fits were made to sparks in all four clusters, and the assumed fiducial positions were displaced to minimize the residuals. The deviations of the new fiducial positions from their survey values averaged 0.8 mm. We then used a beam pion run with the spectrometer magnets turned on, and again trajectories were fit to the sparks in all four counters. Small shifts in fiducial positions were again made, averaging about 0.2 mm.

Most of the shifts required in the effective fiducial positions when the magnet is turned on are explained by a $\vec{V} \times \vec{B}$ deflection of the electrons in the ionized gas. This is most evident in the front cluster where the fringe fields ranged from 40 G at the upstream end to 160 G at the downstream end, and the clearing fields were about 150 V. The expected average shift of the spark positions due to the $\vec{V} \times \vec{B}$ effect is about 0.30 mm, which agrees with the observed average shift of 0.36 mm.

The beam-pion tracks were concentrated in a small region near the center of the chambers, and therefore they were not useful in obtaining information on the rotation angles of the chambers. The alignment parameters which describe the rotations were checked using the low-momentum positive and negative tracks from "Ξ" triggers, which illuminated the chambers more fully. The deviations in the chamber angles found by this method differ from the survey values by about 1 mrad on the average.

In addition to the rotation parameters, the multitrack events are useful in determining effective shifts in the fiducial positions which may be due to the increase in the spark formation time over that for single track events. We are sensitive to spark formation time, since the spark pulse timing is measured relative to the fiducial pulses, which are created at the time the high-voltage pulse is applied to the chamber. The alignment process allowed for this effect, and the shifts observed for multitrack events are about 0.25–0.50 mm. Whenever wands were repaired or remagnetized, or whenever the wand preamplifiers were adjusted or replaced, the performance of the wand changed slightly, and its alignment had to be redetermined. In addition, slow drifts of the alignment parameters were observed, so the data were broken into blocks which were small enough so that the parameters could be treated as constants within each block. In practice, only the fiducial positions were varied from one data block to the next.

The program which performed the final cuts to identify the candidates of interest and to produce the results of the experiment is called POSTAN. The cuts made in this program were on both geometrical and kinematic quantities. We require that the track interpreted as the pion from the "Ξ" decay was distinct from that interpreted as the pion from Λ decay. This was done by demanding that both the vertical and horizontal angles of the two negative tracks in the middle cluster differed by more than 1 mrad, and that their positions differed by more than 0.5 cm in at least one view. We required the extrapolation of the pion from the cascade decay (as seen in the vertical view in the front cluster) to the middle cluster differ from the Λ-decay pion by at least 4 mrad in angle and 1 cm in position. Cuts on the closing distance were also performed for the pion-proton intersection at the Λ vertex and the beam-pion vertex, each of which was required to have a closing distance of less than 3.2 mm. We re-

quired that the beam-pion vertex lie within the fiducial region, which was the 120-cm-long decay region just downstream of the beam chamber. The Λ vertex was required to be downstream of the beam-pion vertex. Finally, a χ^2 cut was made on the fit of the beam track to a trajectory through the hyperon channel, which required that $P(\chi^2) > 2\%$.

To verify that the reconstruction programs functioned properly and to understand the effects of the geometrical and kinematic cuts, the reactions studied in the experiment were generated by a Monte Carlo program. All disintegrations were carried out in the center-of-mass system of the parent particle, assuming an isotropic decay distribution. This distribution was chosen so that any asymmetry observed in the reconstructed Monte Carlo events could be ascribed to an instrumental effect. Each momentum vector was transformed to the laboratory system and traced through the apparatus, requiring that the track be within the acceptance of the experiment and simulating multiple Coulomb scattering whenever it encountered any material. For events which satisfied the acceptance criteria, a record on a "fake" data tape was written. The fake-data tapes were then processed through the chain of analysis programs, and the results were compared with the real data.

In order to conserve computer time, the extended fields of the magnets were simulated in the Monte Carlo program by regions of uniform field in the magnet-shielding and pole-tip regions, with small extra fields added in the region upstream of the front cluster and within both the front and middle clusters. Our estimated uncertainty in the magnetic fields (corresponding roughly to a 0.25% uncertainty in the momentum of a reconstructed track) was simulated by a uniformly distributed jitter in the field value as the event was traced through the magnet. Sparks were generated for each wand, and the effects of efficiency, pulse pair resolution, and spatial resolution were simulated in the generation of these "measured" sparks. These parameters were varied within realistic limits to achieve the best overall simulation of the experimental distributions. Muon background tracks were simulated by generating tracks uniformly distributed in space, slope, and momentum. Either one or zero tracks were generated, giving an average of 0.5 background tracks per event. The beam momentum distribution at the production target was assumed to be uniform, and the beam tracks were traced through the hyperon channel, taking into account the acceptance of the channel and our triggering counters.

The fake data were analyzed with the same pattern-recognition and analysis programs as the real data except that GRIST was modified to use magnetic-field integrals compatible with those used in generating the events. As in the real data, GRIST assumed that there was no bending of tracks due to the fringe field upstream of the front cluster or within the front and middle clusters.

Using the fake-data tape and the actual analysis programs allows a detailed simulation of the effects of spatial and χ^2 cuts and any biases introduced in the fitting procedure. A comparison of the real and fake data shows adequate agreement for most of the distributions we have studied. In cases where disagreements occur, they can be attributed to specific assumptions made about the apparatus, and they are used to help establish our systematic errors. We show in Fig. 2 the momentum distributions for the parent and decay products for reconstructed events passing the criteria for normal decay reaction (3). In Fig. 2(b) we show the difference between the momentum of the cascade as reconstructed from the beam chamber information and from the down-

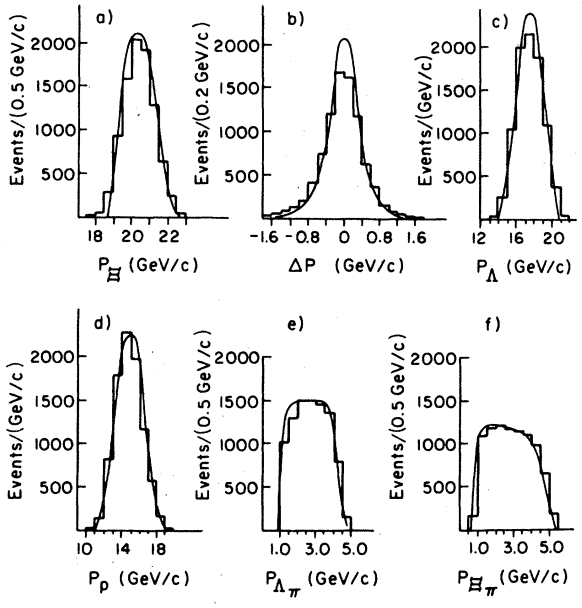

FIG. 2. Momentum distributions of the parent particle and decay products for reconstructed events passing the selection criteria for normal cascade decay, reaction (3). Figure 2(a) shows the momentum of the incident cascade; Fig. 2(b) is the distribution of the difference in momentum of the cascade as reconstructed from the beam channel data and as reconstructed from the momenta of the decay products measured in the spectrometer magnets. Figures 2(c) and (f) are the momenta of the daughter Λ and pion from cascade decay; Figs. 2(d) and (e) are the momenta of the proton and pion from Λ decay. The solid curves are the corresponding distributions obtained from the fake data.

stream spectrometer. Figure 3 shows the vertex distributions along the beam line: (a) X_{Ξ}, cascade vertex, (b) X_{Λ}, Λ vertex, and (c) $X_{\Lambda}-X_{\Xi}$, the Λ decay length. In all of these curves, the solid line represents the corresponding distribution from the fake data.

For the data taken with the "Ξ" trigger or Ξ_{β} trigger, the cuts in TOPSY eliminated all but 25% and 17% of the events, respectively. The events eliminated are primarily decays upstream of the fiducial volume (~70% of all "Ξ" triggers) but include some beam-track interactions and events with poor spark-chamber efficiency. These data were further reduced in GRIST by requiring that the tracks identified by TOPSY fit the topology common to reactions (3) through (6), i.e., the beam particle decaying into a Λ° and a negative track. As GRIST treated the tracks in each of the clusters, it made a least-squares fit to the coordinates of the sparks identified by TOPSY. If the χ^2 was unacceptably large and the track contained more than the minimum number of sparks required to form a track, the spark with the largest deviation was rejected and the track refit. This process was repeated until either the minimum number of sparks was reached and the track was rejected or until a suitable χ^2 was found. The GRIST cuts were made in the following order, and the quantities in parentheses indicate for ("Ξ",Ξ_{β}) triggers the fraction of events surviving the cuts in TOPSY which also survive that cut in GRIST.

(1) Beam vertex. At least one track in the front cluster was required to intersect the beam track within 3.2 mm in the fiducial decay region. Also, tracks whose angles were within 5 mrad of the beam track were not used. This angle cut reduced the background and improved the precision in the determination of the decay vertex (65%, 65%).

(2) Proton. A high-momentum positive track was required to be detected in the middle and rear cluster and to fit a trajectory through the 48D48 with an acceptable χ^2 (49%, 47%).

(3) Λ. The proton track was required to intersect with a negative track which was detected in at least the middle cluster. A continuation of the pion trajectory was searched for in the rear cluster, and, if found, considered part of the pion trajectory. In cases where the Λ appeared to decay upstream of the 72D18, the front cluster sparks were examined for compatibility with the pion or proton trajectories, and, if compatible, added to the appropriate trajectory. For events with a satisfactory geometrical fit for the pion and proton track intersection and with pion-proton effective mass less than 1.130 GeV/c^2, a kinematic fit to the reaction $\Lambda \to p\pi^-$ was made. A

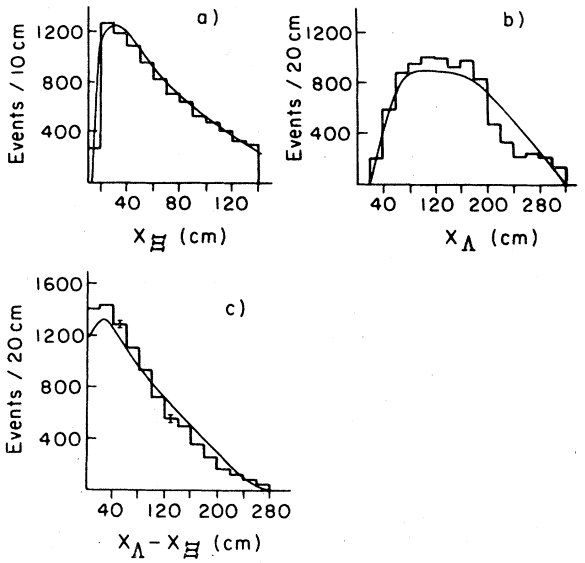

FIG. 3. Distributions of the cascade decay vertex (X_{Ξ}), the Λ decay vertex (X_{Λ}), and the Λ decay length ($X_{\Lambda}-X_{\Xi}$).

loose goodness-of-fit test was made for this kinematic fit (29%, 26%).

(4) Beam $\to \Lambda^{\circ}+X^-$. The Λ trajectory found from the kinematic fit was required to intersect with the beam track. A geometrical fit with this requirement was made, and a cut was applied on the resulting χ^2. A negative track, distinct from the one associated with the Λ vertex was required to be found in the front and middle clusters. This track was required to satisfy a geometrical fit in which it intersected the beam track and the reconstructed Λ momentum vector. This criterion was applied through a goodness-of-fit test on the resulting χ^2 for the geometrical fit (21%, 18%).

In addition to using the fake data, a verification of the pattern recognition and reconstruction programs was made by analyzing two samples of about 20 consecutive "Ξ" triggers both by hand and with the programs. The manual analysis consisted of plotting the sparks to scale and visually interpreting both the track topology and the event type. In this way, we verified that the tracks found by eye were also found by TOPSY, and that our physics interpretation of the event agreed with GRIST. In addition, for a sample of about 150 consecutive "Ξ" triggers, any event which reached step 2 was examined manually. Further detailed checking of more than 100 doubtful $\Xi \to \Lambda\pi$ candidates was done while developing the programs. A few events were found in which misinterpretations had been made by the programs, and these were used to improve the logic of both TOPSY and GRIST.

V. FINAL ANALYSIS AND RESULTS

A. Production ratios

The $F \cdot V$ trigger is our basic normalizing trigger. The bulk of our data taken with this trigger were pions, with only about 1% hyperons but with 10–15% triggers from muons or accidentals. Reconstruction efficiency for a single track in our chambers was quite high, greater than 99%. Thus with high efficiency and negligible background, we identified pions as events with a track found in each cluster, with the track in the beam chamber consistent with a trajectory through the beam channel which intersects the production target. Stray tracks were reduced to a negligible level through these combined momentum and geometrical requirements. The fraction of $F \cdot V$ triggers which were not recognized as pions is shown in Fig. 4 for representative samples of data throughout running periods B and C; we use it to estimate the stability of our normalization against random fluctuations. The nonpion component is relatively stable at $(14 \pm 2)\%$ for the Al_2O_3 (downstream) target and $(10+7)\%$ for the Al (upstream) target. We therefore take the number of pions in our apparatus acceptance as 0.86 times the value of the $F \cdot V$ scaler reading for downstream data and 0.90 $F \cdot V$ for upstream data.

We searched for events which are candidates for reaction (1), normal Σ decay, by examining data taken with the $Y \cdot V$ trigger. Candidates were identified by the requirement that a beam vertex (step 1, above) exist in the fiducial decay region. We find from the analysis of fake data that the efficiency for recognition of events of this type (number found/number generated in the fiducial region) is 0.74 ± 0.05. The ratio of the yield of Σ^- to π^- at the production target is related to the observed rates by the expression

$$\Sigma/\pi = FR_\Sigma/R_\pi \epsilon P\,, \qquad (7)$$

$$P = [1 - \exp(-\Delta/\beta\gamma c\tau)]\exp(-l/\beta\gamma c\tau)$$

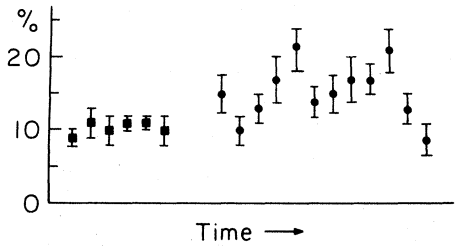

FIG. 4. Fraction of events taken with the $F \cdot V$ trigger which are not recognizable as beam tracks, as a function of run number, or increasing time. The ■ points were taken close together in time, and with the upstream (Al) target. The ● points were taken over a longer time interval and with the downstream (Al_2O_3) target.

in which R_Σ (R_π) is the ratio of Σ vertices (beam tracks) found per $Y \cdot V$ ($F \cdot V$) trigger, $\epsilon = 0.74 \pm 0.05$ is the Σ reconstruction efficiency, F is the ratio of $Y \cdot V$ to $F \cdot V$ trigger rates, l is the effective length of the beam channel, Δ is the length of the fiducial decay region (1.2 m), and τ is the lifetime of the Σ in its rest frame. The values of this ratio were evaluated for two targeting conditions: a downstream Al_2O_3 target, with its center placed approximately 30 cm into the first magnet of the channel and $l = 4.2$ m, and an upstream Al target, with the target placed just upstream of the first channel magnet and $l = 4.5$ m. The mean value of the horizontal production angle for the two target positions are slightly different, and their values are shown in Table I. The vertical production angle is about 1.7 mrad for both configurations. In Table I we give the values for Σ/π for both target conditions for the two running periods B and C, for which we feel the systematic errors and running conditions were sufficiently stable to permit a meaningful measurement of this ratio. The errors on these quantities have been calculated by adding in quadrature the statistical errors for each measurement and our estimate of the fluctuations of the reconstruction efficiency and monitor ratios for each sample. In addition,

TABLE I. Values of the Σ/π ratio at the production target for the two different targeting conditions during the running periods B and C. The momentum of the incident proton beam is 29.4 GeV/c and the central value of the hyperon channel is 20.8 GeV/c. The errors shown for the measurements are a combination of statistical and systematic uncertainties which arise from fluctuations in monitor ratios and spark-chamber performance. The errors on the averages have been enlarged to include other systematic errors, such as uncertainties on the Σ lifetime, the absolute reconstruction efficiency, and the effective channel length. The quantity l is the effective length of the hyperon channel, and θ is the mean horizontal production angle.

Target	$l(m)$	θ (mrad)	Σ/π	Σ/π	Σ/π (average)
Al	4.5	−2.5	1.44 ± 0.19	1.77 ± 0.22	1.57 ± 0.17
Al_2O_3	4.2	5.0	1.02 ± 0.13	1.28 ± 0.15	1.13 ± 0.12

there is an overall systematic error arising from such effects as uncertainties in the average reconstruction efficiency, the Σ^- lifetime, and the effective length of the channel. These latter two uncertainties, amounting to 8%, are added in quadrature to the error after averaging the measurements from periods B and C. Thus the error on the final average values in Table I includes all of our estimates of systematic uncertainty.

To measure the corresponding ratio for cascade production, the same procedure can be followed, except that the evaluation of the reconstruction efficiency is more difficult, due to the very different topology for reaction (3) compared to beam tracks. Following the same procedure as we used for measuring the Σ/π ratio, only using fully reconstructed $\Xi^- \to \Lambda\pi^-$, $\Lambda \to p\pi^-$ in the Ξ trigger, we find the values listed in Table II, under the heading "(Ξ/π) values from method I (full $\Xi^- \to \Lambda\pi^-$ reconstruction)." The overall efficiency for reconstructed $\Xi^- \to \Lambda\pi^-$ found from the analysis of our fake-data events is 0.29 ± 0.10 absolute efficiency or $0.39 \pm .08$ relative to the Σ^- efficiency quoted above (relative efficiencies have smaller systematic errors). The efficiencies are with respect to events entering our fiducial region; the analysis efficiency is ~40% with respect to events satisfying all Ξ^-, Λ fiducial-volume cuts. Because of the problem of determining accurately the reconstruction efficiency, and because it is sensitive to the rate of accidental tracks and the performance of the spark chambers, we have measured the Ξ/π ratio in a second way, which we call method II. In this measurement, we use data from the $Y \cdot V$ triggers (the same data sample as was used in the Σ/π ratio measurements), in which we require both that a beam vertex be found in the decay region (~0.75 efficiency) and that a proton (step 2, above) be found with momentum greater than 10 GeV/c (0.70 ± 0.05 overall efficiency for a beam-π vertex plus a proton). This method is less sensitive to reconstruction efficiency variations (since the ratio of Σ^- to Ξ^- efficiencies is estimated stable to ~3%, more stable than the absolute efficiency uncertainties given above) but it suffers from statistical errors, since only ~2% of $Y \cdot V$ triggers contain cascades which decay in the fiducial region. Taking into account the systematic errors in a similar way to that done for the Σ/π ratio, the two ways of measuring this ratio are seen to be in agreement. We regard the two measurements as independent, and we obtain final values for the Ξ/π ratio by a weighted average of the results of the two methods. In performing the average we have first increased the errors on the individual points by adding our estimates of the uncertainties particular to each method, which is primarily the uncertainty in the absolute reconstruction efficiency, (30% for the full reconstruction, 6% for the indirect method of comparing vertices with protons to Σ^- events) and then added the other systematic errors (uncertainty on the Ξ lifetime and branching ratio and the effective channel length) to the error on the final average.

In order to calculate the branching ratio for the leptonic decay modes, it is necessary to know the ratio of Σ/Ξ in the beam. Since relative rather than absolute reconstruction efficiencies are required, systematic uncertainties are reduced when calculating the Σ/Ξ ratio, and we estimate the ratio by an average of the Σ/Ξ ratios in the different data samples. Systematic relative reconstruction uncertainties of 20% for the full reconstruction Ξ^- sample (from "Ξ") and 3% for the proton signature Ξ^- sample (from $Y \cdot V$ triggers) are included. An 8% uncertainty due to channel length and lifetime uncertainties is included in the error quoted for the extrapolation of the Σ/Ξ ratio back to the production target. Our values for the Σ/Ξ ratios both at the entrance to the fiducial region and at the production target are given in Table III. In the calculation of the leptonic branching ratios in II, we need only the Σ/Ξ ratio at the entrance of the fiducial decay region.

Because of the differences in production target, production angle, beam channel acceptance, and incident proton momentum, it is difficult to compare our results of the production ratios directly with previous measurements of these quantities.[9] However, by making plausible assumptions about the A dependence, θ dependence, and momentum

TABLE II. Values of the Ξ/π ratio at the production target for the targeting conditions given in Table I, using the two different methods described in the text. The errors shown are a combination of statistical and systematic uncertainties as discussed in the text.

Target	$10^3 \times (\Xi/\pi)$ values from method I (full $\Xi^- \to \Lambda\pi^-$ reconstruction) Period B	Period C	Average	$10^3 \times (\Xi/\pi)$ values from method II (vertex in $Y \cdot V$ trigger + proton) Period B	Period C	Average	$10^3 \times (\Xi/\pi)$ (average)
Al	19 ± 7	17 ± 6	18 ± 4.5	23 ± 6	35 ± 7	27 ± 4.5	23 ± 5
Al_2O_3	17 ± 6	19 ± 7	18 ± 4.5	19 ± 7	28 ± 5	2 ± 4.0	22 ± 4

TABLE III. Σ/Ξ ratio measurements. Our best estimate of the Σ/Ξ ratio comes from an average of the ratios in each of the runs and methods in Table II (for Ξ) and Table I (for Σ^-). Since some systematic effects cancel, the Σ/Ξ ratio is more stable and has less fractional systematic uncertainty than the Σ/π and Ξ/π quantities in Tables I and II. Column 1 is the Σ/Ξ ratio in the beam at the entrance to our fiducial region; column 2 is the Σ/π ratio at the production target. The fractional error in the production target ratios is larger because of lifetime and channel-length uncertainties.

Target	Σ/Ξ (fiducial region)	Σ/Ξ (production target)
Al (upstream)	59.0 ± 8	62.0 ± 10
Al_2O_3 (downstream)	47.0 ± 5	49.5 ± 6

dependence,[10] our measurements and previous measurements are in approximate agreement.

B. $\Xi^- \to \Lambda\pi^-$ decay parameter (α_{Ξ^-})

In our analysis for the α decay parameter of the Ξ^-, we assume that the incident Ξ is unpolarized. The justification for this assumption is that the transverse momentum of the Ξ at production is quite small (0.1 GeV/c), and hyperon polarization at high incident proton momentum has been observed only for large transverse momenta.[11] From the data on Λ° polarization, assuming the same mechanism would cause the Ξ to be polarized, we estimate that the polarization of the beam is less than 1%. In addition, the method we have chosen to determine α_{Ξ^-} is insensitive to the incident polarization for a complete sample. While our sample does not cover the full range of Ξ and Λ° decay angles with equal efficiency, we are confident that the effects of a beam polarization of 1% are totally negligible.

In the Λ rest system, the polarization of the Λ is related to the unit vector of the Ξ momentum by the relationship [12]

$$\vec{P}_\Lambda = -\alpha_\Xi \hat{k}_\Xi ,$$

and the decay-angular distribution of the Λ is given by

$$\frac{dN}{d\Omega} = \frac{1}{4\pi}\,(1 + \alpha_\Lambda \vec{P}_\Lambda \cdot \hat{k}_p) = \frac{1}{4\pi}\,(1 - \alpha_\Lambda \alpha_\Xi \hat{k}_\Xi \cdot \hat{k}_p) \tag{8}$$

in which α_Λ is the Λ decay parameter and $\hat{k}_p$ is a unit vector in the direction of the decay proton momentum.

We evaluate experimentally the asymmetry in the distribution of $\hat{k}_\Xi \cdot \hat{k}_p$ in order to determine the quantity $\alpha_\Lambda \alpha_\Xi$. The experimental biases in the apparatus are evaluated using the fake data. Our measurement of the asymmetry, along with the known value of α_Λ yields a measurement of α_{Ξ^-}.

To ensure a clean sample, we use only events from our calibration cascade triggers, with no Čerenkov-counter requirement. Our data sample is 9046 $\Lambda\pi$ events. If we compare the $\Lambda\pi$ mass plot with that generated from the fake data (Fig. 5) we conclude that the background present in this sample is less than 1%, which introduces a negligible effect in the determination of α_Ξ in com-

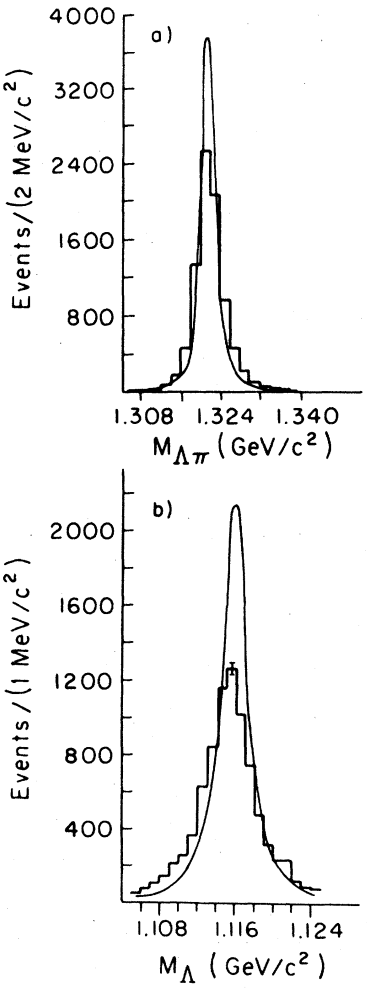

FIG. 5. The $p\pi$ (a) and $\Lambda\pi$ (b) effective-mass distribution for the selected events used in the determination of α_Ξ. The solid curve is the corresponding distribution from the fake data.

parison with our statistical errors. The cuts that we make are not associated in a simple way with the variable $\hat{k}_{\Xi^-} \cdot \hat{k}_p$. However, the combination of the cuts we make does produce an instrumental asymmetry, which we evaluate through the analysis of the fake data. The observed instrumental asymmetry arising in the analysis of the fake-data events is 0.069, compared to 0.367 for the real data. This instrumental correction is not sensitive to the assumed values of such parameters as spark-chamber resolution, pulse-pair resolution, spark-chamber efficiencies, and uncertainties in the magnetic-field values.

Since we depend upon the Monte Carlo program to evaluate our instrumental bias, we have studied several angular distributions in both the cascade and Λ center-of-mass-systems. Figure 6 shows the distribution of the three components of $\hat{k}_p$ (referred to our laboratory coordinate axes) in the Λ center-of-mass system; Fig. 7 shows the distribution of $\hat{k}_\Lambda$ in the cascade center-of-mass system. The coordinate directions are $\hat{x}$, roughly along the beam, $\hat{y}$, the vertical (nonbending) transverse direction, and $\hat{z}$, the horizontal (bending) transverse direction. The dips seen in the y-component distributions of both vectors are related to the loss of close-lying sparks in the spark chambers. Loss of events for negative $\hat{k}_\Lambda \cdot \hat{x}$ is related to a cut excluding pions emitted at small angles (less than 5 mrad) in the decay $\Xi \to \Lambda\pi$. Overall efficiency of the analysis is $\approx 40\%$ of events in the fiducial volume, and the fake-data distributions agree relatively well with the real data. For the real data, there are some correlations between the Λ distributions and the proton distributions, since the real-data decay according to Eq. (8).

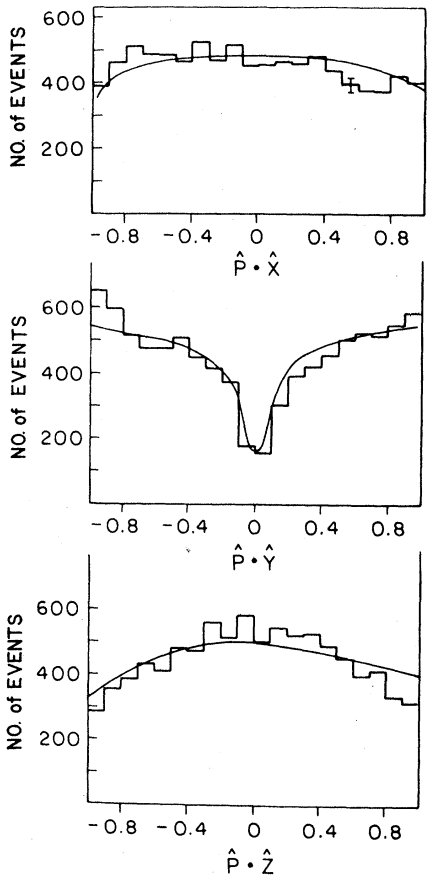

FIG. 6. Distributions of the three components of the proton momentum unit vector in the Λ rest system. The $\hat{x}$, $\hat{y}$, and $\hat{z}$ axes are the fixed laboratory axes. $\hat{x}$ is roughly along the beam direction, $\hat{y}$ is in the vertical direction (nonbending spectrometer plane), and $\hat{z}$ is in the horizontal direction (bending spectrometer plane). The solid curves are the corresponding distributions from the fake data.

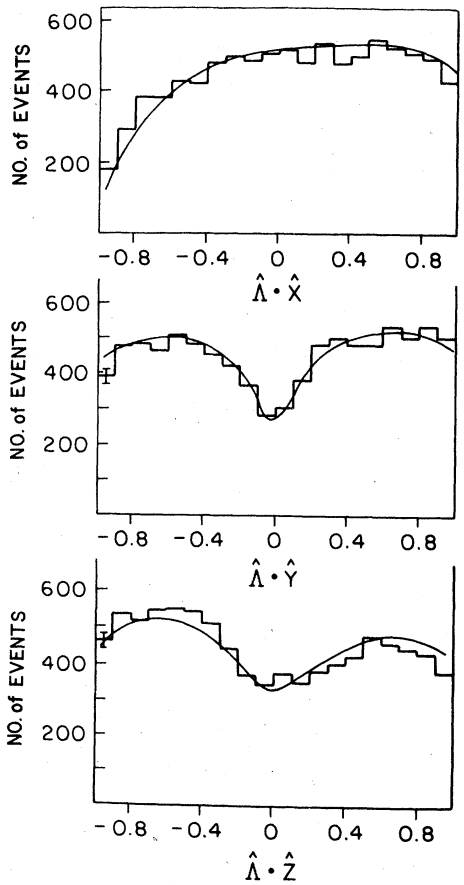

FIG. 7. Distributions of the three components of the Λ-momentum unit vector in the cascade rest system as in Fig. 6, the $\hat{x}$, $\hat{y}$ and $\hat{z}$ axes are the fixed laboratory axes and the solid curves are the corresponding distributions from the fake data.

To form a χ^2 between the fake data and the real data we have weighted the fake-data events according to Eq. (8), using the generated value of $\hat{k}_p \cdot \hat{k}_\Xi$. We have used $\alpha_\Lambda = 0.642$ (the world average)[13] and calculate χ^2 as a function of α_{Ξ^-}. The spatial distributions in Figs. 6 and 7 are sensitive to details of chamber efficiency and analysis cuts but are insensitive to the value of α_{Ξ^-} used [χ^2 of 326/59 degrees of freedom (D.F.) with $\alpha_{\Xi^-} = 0$, χ^2 of 304/59 degrees of freedom with $\alpha_{\Xi^-} = -0.392$, the world average, and $\chi^2 = 300/59$ degrees of freedom with $\alpha_{\Xi^-} = -0.49$, our reported value].

A distribution of the error in the reconstructed $\hat{k}_p \cdot \hat{k}_\Xi$ (evaluated by taking the difference of the reconstructed $\hat{k}_p \cdot \hat{k}_\Xi$ from the generated $\hat{k}_p \cdot \hat{k}_\Xi$ for fake-data events) is shown in Fig. 8. The $\hat{k}_p \cdot \hat{k}_\Xi$ distribution (for real data) is shown in Fig. 9, with a dashed curve showing the fake-data analysis prediction for $\alpha_{\Xi^-} = 0$, and a solid curve showing the prediction with $\alpha_{\Xi^-} = -0.49$, our result. The data in Fig. 9 is shown in bins of 0.1 in $\hat{k}_p \cdot \hat{k}_\Xi$, though bins of 0.2 were used for the final fitting. Our results are insensitive to the difference between these bin sizes. The $\hat{k}_p \cdot \hat{k}_\Xi$ distribution, as we have checked with the fake-data analysis, is insensitive to details of spark-chamber performance and analysis cuts but quite sensitive to α_{Ξ^-} [χ^2 of 218/9 D.F. with $\alpha_{\Xi^-} = 0$, χ^2 of 19.1/9 D.F. with $\alpha_{\Xi^-} = -0.392$ (the world average) and χ^2 of 9.4/9 D.F. with $\alpha_{\Xi^-} = -0.49$].

We have estimated a value for α_{Ξ^-} in two different ways using the difference between the two methods to estimate our systematic error. In Method I, a χ^2 is formed between the fake-data distribution (weighted by $1 - \alpha_{\Xi^-} \hat{k}_p \cdot \hat{k}_\Xi$) and the real data. The parameter α_{Ξ^-} is varied to find the χ^2 minimum (the estimated value of α_{Ξ^-}) and the error on α_{Ξ^-} is the change needed to increase the χ^2 by one. The value of α_{Ξ^-} from this method is $\alpha_{\Xi^-}(\mathrm{I}) = -0.50 \pm 0.035$, with a χ^2 of 9.3 for 9 D.F. In method II, the real data are weighted by the inverse of the distribution of the fake data $\hat{k}_p \cdot \hat{k}_\Xi$, and a fit is made for the asymmetry $\alpha_{\Xi^-} \alpha_\Lambda$ in the resulting weighted distribution. The error is derived from the fit to the weighted distribution; Method II yields $\alpha_{\Xi^-} \alpha_\Lambda = -0.309 \pm 0.018$, or $\alpha_{\Xi^-} = -0.48 \pm 0.028$. The disagreement between methods I and II is 0.02. This difference is consistent with differences in Monte Carlo and real-data asymmetries in Figs. 6 and 7 (center-of-mass distributions of the proton and Λ referred to fixed spatial axes). We then take 0.02 to be an estimate of systematic errors in our experiment. Our final value is then the average of the values from methods I and II, and our reported error is the statistical error added in quadrature to our estimated systematic error:

$$\alpha_{\Xi^-} = -0.49 \pm 0.04 .$$

VI. CONCLUSIONS

A. Production ratios

We have presented values for Σ^-/π^-, Ξ^-/π^-, and Σ^-/Ξ^- production values for Al and Al_2O_3 targets near 0° in the Brookhaven charged-hyperon beam. The proton-beam momentum is 29.4 GeV/c and the hyperons selected are at a mean channel momentum of 20.8 GeV/c. Our results are given in Tables I, II, and III. Under plausible assumptions about dependence upon target, production angle, and momentum, these results are in approximate agreement with those from previous experiments.[9]

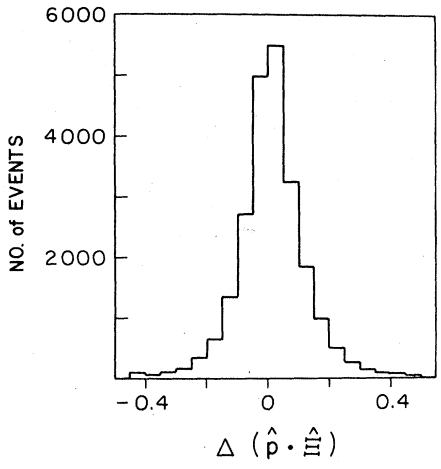

FIG. 8. Distribution of the error on $(\hat{k}_\Xi \cdot \hat{k}_p)$. The error is estimated from the fake data and is the difference of the reconstructed $(\hat{k}_\Xi \cdot \hat{k}_p)$ from the $(\hat{k}_\Xi \cdot \hat{k}_p)$ as it is generated.

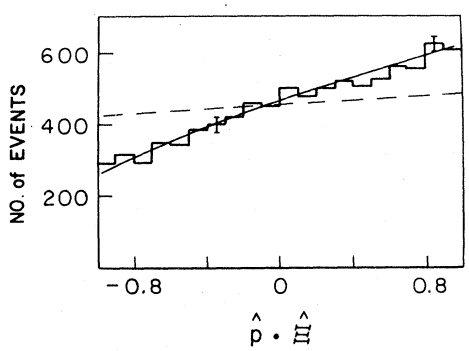

FIG. 9. Distribution of the quantity $(\hat{k}_\Xi \cdot \hat{k}_p)$ c.m. from which the determination of α_{Ξ^-} is made. The solid line is the fitted curve from which the asymmetry is determined. The dashed line is the fake data generated with the assumption that $\alpha_{\Xi^-} = 0$, and indicates the size of the instrumental asymmetry.

B. $\Xi^- \to \Lambda\pi^-$ decay parameter (α_{Ξ^-})

Our result $\alpha_{\Xi^-} = -0.49 \pm 0.04$ is somewhat higher than, but consistent with, the previous world average of α_{Ξ^-} (Ref. 13). It is consistent with the world average[12] of α_{Ξ^0} and thus consistent with the $\Delta I = \frac{1}{2}$ rule which predicts $\alpha_{\Xi^-} = \alpha_{\Xi^0}$ (no phase-space corrections) or $\alpha_{\Xi^0} = 0.975\alpha_{\Xi^-}$ (phase-space corrections included). A summary of these values is given in Table IV.

TABLE IV. Values of the asymmetry parameter in $\Xi^- \to \Lambda\pi^-$ decay.

	Ref.	Value
α_{Ξ^-}, world average	12	-0.392 ± 0.021
α_{Ξ^0}, world average	13	-0.478 ± 0.034
α_{Ξ^-}, this experiment		-0.49 ± 0.04

*Present address: Physics Department, University of Pennsylvania, Philadelphia, Pennsylvania 19104.
†Present address: Singer Co., Kearfott Division, 150 Totowa Rd., Wayne, New Jersey 07470

[1]J. A. Thompson *et al.*, following paper, Phys. Rev. D 21, 25 (1980), referred to hereafter as II. For further details, see M. L. Herbert, Ph.D. thesis, University of Pittsburgh, 1978 (unpublished).
[2]V. Hungerbühler *et al.*, Nucl. Instrum. Methods 115, 221 (1974).
[3]W. J. Willis *et al.*, Nucl. Instrum. Methods 91, 33 (1971).
[4]K. J. Foley *et al.*, Nucl. Instrum. Methods 108, 33 (1973).
[5]E. F. McLaughlin *et al.*, Nucl. Instrum. Methods 70, 343 (1969).
[6]D. Freytag, Nucl. Instrum. Methods 138, 685 (1976).
[7]V. L. Highland and R. J. Macek, Nucl. Instrum. Methods 64, 69 (1968).
[8]D. I. Lowenstein, Nucl. Instrum. Methods 109, 589 (1973).
[9]J. Badier *et al.*, Phys. Lett. 39B, 414 (1972); V. Hungerbühler *et al.*, Phys. Rev. Lett. 30, 1234 (1973).
[10]J. Lach, private communication.
[11]K. Heller *et al.*, Phys. Lett. 68B, 480 (1977).
[12]G. Bunce *et al.*, Phys. Rev. D 18, 633 (1978).
[13]Particle Data Group, Phys. Lett. 75B, 1, (1978).